Inorg. Chem. **2007**, *46*, 6516–6528

Synthesis, Characterization, Solid-State Structures, and Spectroscopic Properties of Two Catechol-Based Luminescent Chemosensors for Biologically Relevant Oxometalates

Helen D. Batey, Adrian C. Whitwood, and Anne-K. Duhme-Klair*

Department of Chemistry, University of York, Heslington, York YO10 5DD, U.K.

Received March 23, 2007

The new heteroditopic ligand 2,3-dihydroxy-*N*-(1,10-phenanthroline-5-yl)benzamide (**H$_2$-L^3**) was synthesized and coordinated to [Ru(bpy)$_2$(phen)]$^{2+}$- and [ReBr(CO)$_3$(phen)]-type luminophores (bpy = 2,2′-bipyridine and phen = 1,10-phenanthroline). The resulting chemosensors [Ru(bpy)$_2$(**H$_2$-L^3**)]$^{2+}$ and [ReBr(CO)$_3$(**H$_2$-L^3**)] were fully characterized and their solid-state structures and spectroscopic properties were investigated to assess how the photophysical properties of the luminescent signaling units affect the performance of the sensors. [Ru(bpy)$_2$(**H$_2$-L^3**)]$^{2+}$ and [ReBr(CO)$_3$(**H$_2$-L^3**)] both signal the presence and concentration of molybdate and vanadate in aqueous acetonitrile through a decrease in emission intensity. [ReBr(CO)$_3$(**H$_2$-L^3**)] also detects tungstate. Due to the higher emission intensity of the Ru-based sensor, its detection limits for molybdate (43 μg L^{-1}) and vanadate (24 μg L^{-1}) are almost 1 order of magnitude lower than the ones achieved with the Re-based sensor. The optimum working pH of the chemosensors is determined by the pK_a values of the 2-hydroxy-groups of the receptor units: pH 4 for [ReBr(CO)$_3$(**H$_2$-L^3**)] and pH 3 for [Ru(bpy)$_2$(**H$_2$-L^3**)]$^{2+}$. Both sensors are selective: equimolar amounts of PO_4^{3-}, SO_4^{2-}, ReO_4^-, Mn(II), Fe(III), Co(II), Ni(II), Cu(II), and Zn(II) do not interfere with the detection of molybdate or vanadate.

Introduction

Recent advances in the field of oxoanion recognition have led to the development of a new range of selective chemosensors.[1] The commonest oxoanions targeted are nitrate, sulfate, phosphate, and phosphate derivatives, including ATP^{n-}.[2] Studies addressing the structurally related oxometalates molybdate, tungstate or vanadate, however, are still rare.[3] Despite the biological,[4,5] industrial,[6] and environmental importance[7] of such species, there are, as yet, no luminescent chemosensors for oxometalates on the market.[8]

Most receptor units for oxoanions are designed to take advantage of host−guest interactions, such as hydrogen bonding and electrostatic attraction.[1,2] A supramolecular approach, however, makes it difficult to differentiate oxometalates, such as MoO_4^{2-} and HVO_4^{2-}, from oxoanions of similar size, shape, and charge, such as SO_4^{2-} and HPO_4^{2-}. Coordination chemistry, on the other hand, can be used to achieve the required selectivity since the metal centers in MoO_4^{2-}, WO_4^{2-}, and HVO_4^{2-} are able to bind additional ligands to enhance their coordination number to six (Scheme 1). SO_4^{2-} and HPO_4^{2-} cannot react in this way.

In our recent research, we thus based the selectivity of our sensor molecules on a combination of coordinative bonding and electrostatics by choosing 2,3-dihydroxybenzamides (catecholamides) as receptor units.[9] Catechols are known to react with oxometalates.[10−12] Once deprotonated, the negatively charged O donors have a high affinity for hard, highly charged metal ions.[13] Selectivity for oxometalates over cations can be achieved by pH control, since the pH dependence of the reaction of oxometalates with catechols is fundamentally different from the binding of cations (Scheme 1).

* To whom correspondence should be addressed. E-mail: akd1@york.ac.uk.

(1) (a) Beer, P. D.; Gale, P. A. *Angew. Chem., Int. Ed.* **2001**, *40*, 486. (b) Gale, P. A. *Coord. Chem. Rev.* **2003**, *240*, 1.
(2) Fabbrizzi, L.; Licchelli, M.; Rabaioli, G.; Taglietti, A. *Coord. Chem. Rev.* **2000**, *205*, 85.
(3) (a) Pal, B. K.; Singh, K. A.; Dutta, K. *Talanta* **1992**, *39*, 971. (b) Kawakubo, S.; Suzuki, H.; Iwatsuki, M. *Anal. Sci.* **1996**, *12*, 767. (c) Jiang, C.; Wang, J.; He, F. *Anal. Chim. Acta* **2001**, *439*, 307 and references therein.
(4) Pau, R. N.; Lawson D. M. In *Metal Ions in Biological Systems*; Sigel, H., Sigel, A., Eds.; Marcel Dekker: New York, 2002; p 32.
(5) Kuper, J.; Llamas, A.; Hecht, H.-J.; Mendel, R. R.; Schwarz, G. *Nature* **2004**, *430*, 803.
(6) (a) Sato, K.; Aoki, A.; Noyori, R. *Science* **1998**, *281*, 1646. (b) Sato, K.; Aoki, A.; Takagi, T.; Noyori, R. *J. Am. Chem. Soc.* **1997**, *119*, 12386.
(7) Pyrzynska, K.; Wierzbicki, T. *Talanta* **2004**, *64*, 823.
(8) Haugland, R. P. *Handbook of Fluorescent Probes and Research Products;* Molecular Probes, 2004. http://www.probes.com.

10.1021/ic700554n CCC: $37.00 © 2007 American Chemical Society
Published on Web 07/06/2007

Scheme 1

$$MoO_4^{2-} + 2H_2cat \rightleftharpoons [MoO_2(cat)_2]^{2-} + 2H_2O$$

$$Fe^{3+} + 3H_2cat \rightleftharpoons [Fe(cat)_3]^{3-} + 6H^+$$

Protocols for the quantitative analysis of molybdate based on the colorimetric detection of its catecholate complexes are well established.[14] The sensitivity of these techniques, however, is limited to the micromolar range by the low intensity of the characteristic ligand-to-metal charge-transfer band. In order to develop a more sensitive fluorimetric technique, we are interested in luminescent signaling units with high quantum yields and their ability to signal recognition events at appended catechol units via photoinduced electron-transfer processes or excited-state switching.

Catechol units that are linked to luminescent signaling units have previously been shown to function as sensors,[15−17] redox switches,[18] and photo-[19] and electrocatalysts.[20] $[Ru(bpy)_3]^{2+}$-type luminophores are the most commonly studied; however, $[ReX(CO)_3(bpy)]$-type luminophores (with bpy = 2,2′-bipyridine and X = Br, Cl) are beginning to appear more frequently in the field.[21−24] In addition, complexes with functionalized 1,10-phenanthroline ligands are being developed.[25−27] These often have significantly higher emission quantum yields and lifetimes than corresponding bipyridine-based systems.[28]

In our previous work, we connected catechols as receptor units to $[Ru(bpy)_3]^{2+}$- and $[Re(CO)_3(bpy)(py)]^+$-type luminophores to obtain molecular sensors **1** and **2**, which signal the presence and concentration of oxometalates in solution through a decrease in emission intensity.[9] The high selectivity of **1** and **2** for molybdate is consistent with the recent finding that the siderophore aminochelin [*N*-(2, 3-dihydroxybenzoyl)-diaminobutane] of *Azotobacter vinelandii*, which was used as the molybdenum-binding unit in our first sensor prototype (**1**),[9a] is potentially a "molybdophore".[29]

In this paper, we describe the synthesis and the properties of two new molecular sensors, **3** and **4**, which are based on 2,3-dihydroxy-*N*-(1,10-phenanthroline-5-yl)benzamide ($\mathbf{H_2}$-$\mathbf{L^3}$), a ligand suitable for coordination to $[Ru(bpy)_2]^{2+}$ as well as $[ReX(CO)_3]$ fragments. $\mathbf{H_2}$-$\mathbf{L^3}$ was designed to allow a systematic investigation of the effect of the photophysical properties of the luminescent signaling unit on the performance of the chemosensors.

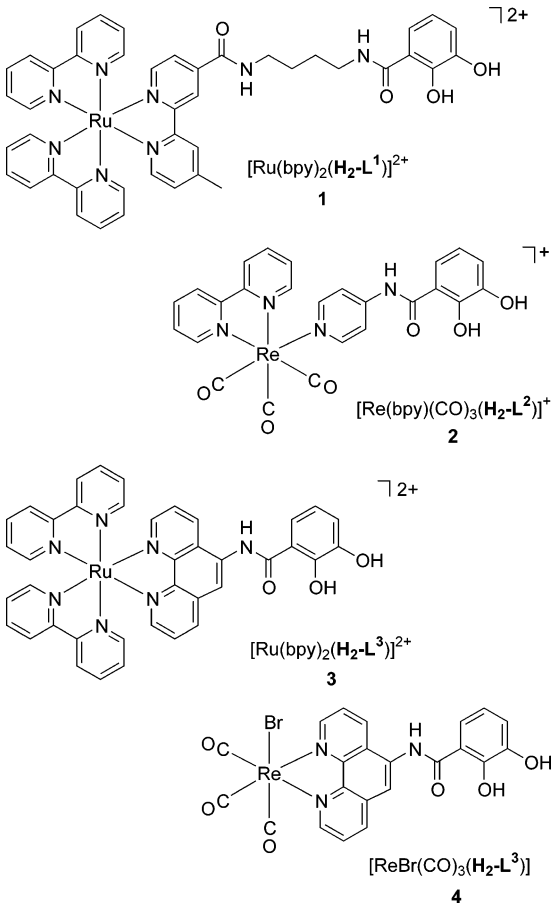

Experimental Section

Reagents and Instrumentation. Commercially available reagents were obtained from Aldrich, Fluka, or Lancaster and used as supplied. Solvents were dried over molecular sieves where necessary. NMR spectra were recorded on Jeol JNM-EX270 or Bruker AMX500 instruments. Absorption spectra were measured on a Hitachi U-300 spectrophotometer in 10 mm quartz cuvettes. The emission and excitation spectra were recorded on a Hitachi F-4500 fluorimeter and are uncorrected. The pH measurements were carried out by using a WTW Profilab pH 597 pH meter equipped

(9) (a) Jedner, S. B.; James, R. J.; Perutz, R. N.; Duhme-Klair, A.-K. *J. Chem. Soc., Dalton Trans.* **2001**, 2327. (b) Jedner, S. B.; Perutz, R. N.; Duhme-Klair, A.-K. *Z. Anorg. Allg. Chem.* **2003**, *629*, 2421. (c) Peacock, A. F. A.; Batey, H. D.; Raendler, C.; Whitwood, A. C.; Perutz, R. N.; Duhme-Klair, A.-K. *Angew. Chem., Int. Ed.* **2005**, *44*, 1712.
(10) Kustin, K.; Liu, S.-T. *J. Am. Chem. Soc.* **1973**, *95*, 2487.
(11) Duhme-Klair, A.-K.; Vollmer, G.; Mars, C.; Fröhlich, R. *Angew. Chem., Int. Ed.* **2000**, *39*, 1626.
(12) Liu, C.-M.; Nordlander, E.; Schmeh, D.; Shoemaker, R.; Pierpont, C. G. *Inorg. Chem.* **2004**, *43*, 2114.
(13) (a) Pierpont, C. G.; Buchanan, R. M. *Coord. Chem. Rev.* **1981**, *38*, 45. (b) Pierpont, C. G.; Lange, C. W. *Prog. Inorg. Chem.* **1994**, *41*, 331.
(14) Snell, F. D. *Photometric and Fluorometric Methods of Analysis, Metals Part 2*; John Wiley & Sons: New York, 1978; p 1296.
(15) Beer, P. D. *Chem. Commun.* **1996**, 689.
(16) Costa, I.; Fabbrizzi, L.; Pallavicini, P.; Poggi, A.; Zani, A. *Inorg. Chim. Acta* **1998**, *275*−*276*, 117.
(17) O'Bian, L.; Duati, M.; Rau, S.; Guckian, A. L.; Keyes, T. E.; O'Boyle, N. M.; Serr, A.; Görls, H.; Vos, J. G. *J. Chem. Soc., Dalton Trans.* **2004**, 514.
(18) Goulle, V.; Harriman, A.; Lehn, J.-M. *J. Chem. Soc., Chem. Commun.* **1993**, 1034.
(19) (a) Whittle, B.; Everest, N. S.; Howard, C.; Ward, M. D. *Inorg. Chem.* **1995**, *34*, 2025. (b) Shukla, A. D.; Whittle, B.; Bajaj, H. C.; Das, A.; Ward, M. D. *Inorg. Chim. Acta* **1999**, *285*, 89.
(20) Storrier, G. D.; Takada, K.; Abruna, H. D. *Inorg. Chem.* **1999**, *38*, 559.
(21) Schanze, K. S.; MacQueen, D. B.; Perkins, T. A.; Cabana, L. A. *Coord. Chem. Rev.* **1993**, *122*, 63.
(22) Sun, S.-S.; Lees, A. J. *Coord. Chem. Rev.* **2002**, *230*, 171.
(23) Lewis, J. D.; Perutz, R. N.; Moore, J. N. *Chem. Commun.* **2000**, 1865.
(24) Busby, M.; Matousek, P.; Towrie, M.; Clark, I. P.; Motevalli, M.; Hartl, F.; Vlček, A., Jr. *Inorg. Chem.* **2004**, *43*, 4523.
(25) Bai, G.-Y.; Wang, K.-Z.; Duan, Z.-M.; Gao, L.-H. *J. Inorg. Biochem.* **2004**, *98*, 1017.
(26) Lazarides, T.; Miller, T. A.; Jeffery, J. C.; Ronson, T. K.; Adams, H.; Ward, M. D. *Dalton Trans.* **2005**, 528.
(27) Higgins, B.; DeGraff, B. A. *Inorg. Chem.* **2005**, *44*, 6662.
(28) Kober, E. M.; Meyer, T. J. *Inorg. Chem.* **1985**, *24*, 106.
(29) Liermann, L. J.; Guynn, R. L.; Anbar, A.; Brantley, S. L. *Chem. Geol.* **2005**, *220*, 285.

with a Metler Toledo InLab 422 pH electrode. The pH scale was calibrated by using Gran's method.[30] Infrared spectra were recorded on a Perkin-Elmer Lambda 7 FT-IR instrument. Electrospray ionization mass spectra were obtained using a Finnigan LCT mass spectrometer and CI and EI mass spectra were measured on a VG Analytical Autospec mass spectrometer. HR-mass spectra were obtained from the EPSRC National Mass Spectrometry Service Centre in Swansea. Elemental analyses were performed by the analytical services at the University of Manchester. Diffraction data were collected on a Bruker Smart Apex diffractometer with an Oxford cryostream cooling system and Mo Kα radiation source using a SMART CCD camera. Structures were solved by direct methods using *SHELXS-97* and refined by full-matrix least-squares using *SHELXL-97* (G. M. Sheldrick, University of Göttingen, Germany, 1997). All non-hydrogen atoms were refined anisotropically. Hydrogen atoms were placed using a riding model and included in the refinement at calculated positions.

Synthesis of 2,3-Dimethoxy-*N*-(1,10-phenanthroline-5-yl)benzamide, Me_2-L^3. Dicyclohexylcarbodiimide (1.13 g, 5.5 mmol) was added at 0 °C to a stirred solution of 2,3-dimethoxybenzoic acid (2.00 g, 11.0 mmol) in 50 mL of dry acetonitrile. After 15 min, the reaction was brought to room temperature and stirred until thin-layer chromatography (TLC) analysis (10:1 chloroform/methanol v/v) confirmed that the reaction had gone to completion. After removal of the precipitated byproduct by filtration, the filtrate was evaporated to dryness. 2,3-Dimethoxybenzoic anhydride was obtained as an oily residue, which was redissolved in 20 mL anhydrous acetonitrile. 1,10-Phenanthroline-5-yl amine (0.80 g, 4.1 mmol) was suspended in 50 mL anhydrous chloroform, and the insoluble components were removed by filtration. The resulting solution was added to the 2,3-dimethoxybenzoic anhydride solution, and the mixture was refluxed for 6 h under N_2 and under exclusion of light. After the removal of the solvents, the residual oil was taken up in chloroform. The product was extracted from the organic phase with 2 M HCl. The pH of the aqueous phase was then increased to 10 with 3 M NaOH, and the product was re-extracted into chloroform. The solvent was removed in vacuo, and the remaining white solid was vacuum-dried. Recrystallization from chloroform/petroleum ether gave the pure product. Yield: 1.23 g (3.4 mmol, 83%). ^{1}H NMR (500 MHz, CD_3CN): δ 10.511 (s, 1H, N*H*), 9.155 (d, 1H, phen C*H*), 9.042 (d, 1H, phen C*H*), 8.605 (s, 1H, phen C*H*), 8.515 (d, 1H, phen C*H*), 8.356 (d, 1H, phen C*H*), 7.804 (m, 1H, phen C*H*), 7.679 (m, 2H, 1 phen C*H*, 1 cat C*H*), 7.274 (m, 2H, cat C*H*), 4.089 (s, 3H, CH_3), 3.953 (s, 3H, CH_3). ^{13}C NMR (125 MHz, CD_3CN): δ 165.2 (*C*═O), 150.9 (phen *C*H), 150.3 (phen *C*H), 136.8 (phen *C*H), 131.0 (phen *C*H), 125.6 (cat *C*H), 124.5 (cat *C*H), 124.1 (phen *C*H), 123.1 (phen *C*H), 119.4 (phen *C*H), 117.4 (cat *C*H), 62.4 (−O−CH_3), 56.9 (−O*C*H3). UV−vis (CH_3CN/H_2O 20:1): $\epsilon_{270\ nm}$ = 26 000 dm^3 mol^{-1} cm^{-1}. Mp: 108−110 °C. HR-CI−MS: *m*/*z* 360.1347 (calculated for $C_{21}H_{18}N_3O_3$: 360.1348).

Synthesis of $[Ru(bpy)_2(Me_2$-$L^3)](PF_6)_2$. Under an inert atmosphere, Me_2-L^3 (0.20 g, 0.55 mmol) and *cis*-$[RuCl_2(bpy)_2] \times 2H_2O$ (0.25 g, 0.55 mmol) were dissolved in 35 mL of a EtOH/H_2O 3:1 mixture and refluxed for 6 h. After cooling, the volume of the solution was reduced by half, and the product was precipitated by the addition of a saturated solution of ammonium hexafluorophosphate in water. The precipitate was isolated, washed with cold water and ethanol, and dried in vacuo. Yield: 0.51 g (0.47 mmol, 94%). ^{1}H NMR (500 MHz, CD_3CN): δ 10.90 (s, 1H, N*H*), 9.07 (s, 1H, phen C*H*), 8.68 (d, 1H, phen C*H*), 8.61 (d, 1H, phen C*H*), 8.53 (m, 4H, bpy C*H*), 8.17 (d, 1H, phen C*H*), 8.11 (m, 2H, bpy C*H*), 8.01 (m, 3H, bpy C*H* and phen C*H*), 7.84 (m, 3H, bpy C*H* and phen C*H*), 7.72 (m, 3H, phen C*H* and cat C*H*), 7.58 (m, 2H, bpy C*H*), 7.46 (m, 2H, bpy C*H*), 7.32 (m, 2H, cat C*H*), 7.26 (m, 2H, bpy C*H*), 3.93 (s, 6H, CH_3). ^{13}C NMR (125 MHz, CD_3CN): δ 165.4 (*C*═O), 153.9 (*C*H bpy), 153.6 (*C*H phen), 153.0 (*C*H bpy), 152.3 (*C*H phen), 138.9 (*C*H bpy), 137.4 (*C*H phen), 132.1(*C*H phen), 128.6 (*C*H bpy), 128.4 (*C*H bpy), 127.3 (*C*H cat), 127.0 (*C*H phen), 126.0 (*C*H cat), 125.3 (*C*H bpy), 123.1 (*C*H cat), 118.6 (*C*H phen), 117.9 (*C*H phen), 62.6 (−O*C*H$_3$), 56.9 (−O*C*H$_3$). UV−vis (CH_3CN/H_2O 20:1): $\epsilon_{450\ nm}$ =16 500 dm^3 mol^{-1} cm^{-1}. Mp: 274−276 °C. HR-ESI-MS: *m*/*z* 912.1357 (calculated for $C_{41}H_{33}O_3N_7F_6P_{96}Ru$: 912.1358).

Synthesis of $[Ru(bpy)_2(H_2$-$L^3)](PF_6)_2$, 3 $(PF_6)_2$. Under an inert atmosphere, $[Ru(bpy)_2(Me_2$-$L^3)](PF_6)_2$ (0.25 g, 0.24 mmol) was dissolved in 15 mL anhydrous dichloromethane. The solution was cooled to −78 °C, and a 10-fold molar excess of 1.0 M boron tribromide in dichloromethane was added slowly. The reaction was stirred at −78 °C for 1 h and then allowed to warm to room temperature over 12 h. Water was added carefully until no more HBr evolved. The mixture was evaporated to dryness, and the residue was taken up in methanol, which was evaporated to remove boron-containing byproducts. The residue was then dissolved in a minimum amount of methanol, and the solution was brought to neutral pH with 3 M NaOH to precipitate the product. To ensure that all **3** precipitated, a few drops of a saturated ammonium hexafluorophosphate solution were added and the mixture was cooled to 4 °C for 12 h. The precipitate was isolated, washed with cold water, and dried in vacuo. Yield: 0.17 g (0.16 mmol, 68%). ^{1}H NMR (500 MHz, CD_3CN): δ 8.923 (d, 1H, phen C*H*), 8.695 (m, 2H, phen C*H*), 8.534 (m, 5H, bpy C*H*), 8.160 (m, 2H, phen C*H*), 8.107 (m, 2H, bpy C*H*), 8.014 (m, 4H, bpy C*H*), 7.841 (m, 3H bpy C*H* and phen C*H*), 7.741 (m, 1H, phen C*H*, 7.31 (d, 1H, cat C*H*), 7.584 (d, 1H, cat C*H*), 7.465 (m, 2H, bpy C*H*), 7.286 (m, 2H, bpy C*H* and cat C*H*). ^{13}C NMR (125 MHz, CD_3CN): δ 170.0 (*C*═O), 154.5 (phen *C*H), 154.4 (phen *C*H), 153.2 (cat *C*H), 153.0 (cat *C*H), 153.9 (bpy *C*H), 141.1 (bpy *C*H), 138.9 (bpy *C*H), 138.2 (phen *C*H), 134.8 (phen *C*H), 131.5 (phen *C*H), 128.6 (bpy *C*H), 128.5 (cat *C*H), 127.9 (phen *C*H), 127.6 (phen *C*H), 125.3 (bpy *C*H). UV−vis (CH_3CN/H_2O, 20:1; pH 6): $\epsilon_{450\ nm}$ = 17 100 dm^3 mol^{-1} cm^{-1}. Mp: 279−280 °C. HR-ESI-MS: *m*/*z* = 890.1012 (calculated for $C_{39}H_{29}O_3N_7F_6P_{102}Ru$: 890.1012).

Synthesis of $[ReBr(CO)_3(Me_2$-$L^3)]$. Me_2-L^3 (0.34 g, 0.94 mmol) and rhenium pentacarbonyl bromide (0.19 g, 0.46 mmol) were dissolved in 80 mL dry toluene and refluxed for 4 h under an inert atmosphere. Once the completeness of the reaction was confirmed by IR spectroscopy, the volume of the reaction mixture was reduced to half. A yellow precipitate formed, which was isolated, washed with cold toluene, and dried. Yield: 0.29 g (0.41 mmol, 90%). ^{1}H NMR*:* (500 MHz, $CDCl_3$): δ 11.104 (s, 1H, N*H*), 9.460 (d, 1H, phen C*H*), 9.286 (d, 1H, phen C*H*), 9.143 (s, 1H, phen C*H*), 8.666 (d, 1H, phen C*H*), 8.505 (d, 1H, phen C*H*), 7.911 (m, 1H, phen C*H*), 7.866 (d, 1H, cat C*H*), 7.816 (m, 1H, phen C*H*), 7.364 (t, 1H, cat C*H*), 7.209 (d, 1H, cat C*H*), 4.101 (s, 3H, CH_3), 3.993 (s, 3H, OCH_3). ^{13}C NMR (125 MHz, $CDCl_3$): δ 196.6 (Re−*C*O), 163.9 (*C*═O), 153.1 (phen *C*H), 152.0 (phen *C*H), 137.8 (phen *C*H), 131.0 (phen *C*H), 126.2 (phen *C*H), 125.6 (phen *C*H), 125.5 (cat *C*H), 123.2 (cat *C*H), 116.9 (cat *C*H), 116.5 (phen *C*H), 62.4 (−OCH_3), 56.4 (−OCH_3). UV−vis (CH_3CN/H_2O, 20:1): $\epsilon_{390\ nm}$ = 3140 dm^3 mol^{-1} cm^{-1}. IR (THF): ν(CO) 2019, 1918, 1893 cm^{-1}. Mp: 248−250 °C. HR-FAB-MS: *m*/*z* 686.0240 (calculated for $C_{24}H_{17}N_3O_6{}^{185}Re$ Na: 686.0233).

(30) Gran, G. *Analyst* **1952**, *77*, 661.

Scheme 2

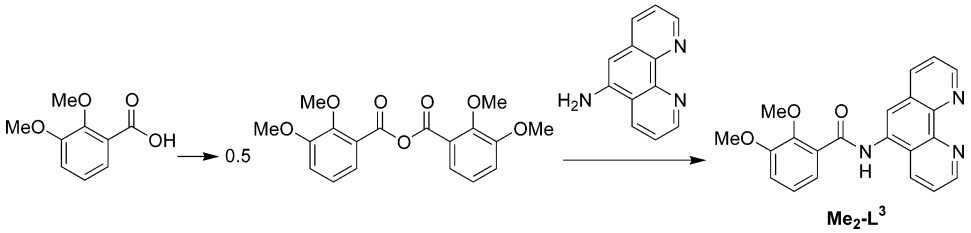

Me_2-L^3

N.B.: [ReCl(CO)$_3$(**Me_2-L^3**)] can be synthesized from rhenium pentacarbonyl chloride, analogue to the procedure described for [ReBr(CO)$_3$(**Me_2-L^3**)]. Upon deprotection with BBr_3, however, a partial exchange of the chloride ligands with bromide ligands was observed.

Synthesis of [ReBr(CO)$_3$(H_2-L^3)], 4. Under an inert atmosphere, [ReBr(CO)$_3$(**Me_2-L^3**)] (0.20 g, 0.029 mmol) was dissolved in 15 mL anhydrous dichloromethane and cooled to −78 °C. A 10-fold molar excess of 1.0 M boron tribromide in dichloromethane was slowly added. The reaction was stirred at −78 °C for 1 h and then allowed to warm to room temperature. The mixture was stirred at room temperature for a further 12 h. Water was added until additions no longer caused the evolution of HBr. The reaction mixture was evaporated to dryness, and the residue was taken up in methanol (approximately 200 mL). The volume of the solution was reduced until a yellow precipitate formed, which was isolated and vacuum-dried. Yield: 0.14 g (0.21 mmol, 72%). ^{1}H NMR (500 MHz, CD_3CN): δ 11.37 (s, 1H, O*H*), 9.77 (s, 1H, O*H*), 9.46 (d, 1H, phen C*H*), 9.39 (d, 1H, phen C*H*), 8.82 (d, 1H, phen C*H*), 8.75 (d, 1H, phen C*H*), 8.46 (s, 1H, phen C*H*), 7.97 (m, 2H, phen C*H*), 7.57 (d, 1H, cat C*H*), 7.15 (d, 1H, cat C*H*), 6.97 (m, 2H, cat C*H* and N*H*). IR (CH_3CN): ν(CO) 2022, 1918 and 1896 cm^{-1}. Mp: 263−265 °C. Elemental Anal. Calcd for $C_{22}H_{13}O_6N_3ReBr$: C, 38.5; H, 2.2; N, 5.8. Found: C, 38.7; H, 1.8; N, 6.1.

General Titration Protocol. The solvent system used consisted of a mixture of acetonitrile and water in 20:1 ratio. Adjustments to the pH were carried out with a 0.6 M solution of HCl in this solvent system and a 0.6 M solution of tetramethyl ammonium hydroxide in water. Solutions of ruthenium-based compounds were made to a concentration of 0.02 mM, and rhenium-based compounds were made to a concentration of 0.1 mM. These concentrations gave an absorbance within the Beer−Lambert range. For the ruthenium-based samples, the excitation wavelength was set to 450 nm and uncorrected spectra were recorded between 490 and 800 nm. The rhenium-based samples were excited at 390 nm, and uncorrected spectra were recorded between 450 and 800 nm. In all cases, 3 mL amounts of the solutions were pipetted into a 10 mm quartz cuvette, which remained sealed to minimize solvent evaporation.

Determination of pH Profiles. The solution of the sensors was adjusted to the starting pH value using the standard acid or base solution, and a spectrum was recorded. Depending on the direction of the titration, small aliquots of either acid or base were added to the sample. The pH of the solution was allowed to stabilize before a spectrum was recorded. The spectra were recorded at intervals of approximately 0.5 pH units, across the pH range of ca. 1−10. Analogous titrations were conducted in the presence of stoichiometric quantities of the oxometalates of interest as well as potentially interfering anions and cations. For this purpose, aqueous standard solutions of the corresponding metal salts were added in stoichiometric quantities in a 5 μL aliquot, so as not to significantly alter the solvent composition. Standard solutions of oxoanions were prepared by using $Na_2MoO_4 \cdot 2H_2O$, $Na_2WO_4 \cdot 2H_2O$, NH_4VO_3, NH_4ReO_4, Na_2SO_4, and Na_2HPO_4. Metal cations were used as chloride or nitrate salts.

Metal-to-Sensor Titrations. Titrations for the determination of the composition of the complexes were conducted using the following procedure. A volume of 3 mL of the sample was buffered with 3.6 μL of lutidine, and the pH was adjusted to the required value with standard acid and base solutions. To the 0.02 mM solution of [Ru(bpy)$_2$(**H_2-L^3**)]$^{2+}$, 5 μL aliquots of a metal-containing solution of concentration 0.75 mM were added. After each addition, the sample was stirred for ca. 3 min to allow the solution to equilibrate before the emission spectrum was recorded. Aliquots of the metal-containing solution were added until an approximate 1:1 ratio was reached. For the analogous titrations with [ReBr(CO)$_3$(**H_2-L^3**)], the sample solutions were 0.1 mM and the solutions of metal salts were 3.75 M.

Competitive Selectivity. To test the selectivity of the sensors, their emission intensity at λ_{max} was recorded in the absence and presence of each potentially interfering ion. The experiments were conducted at a pH value, which was within the active range of the particular sensor. First, the emission intensity of the free sensors was recorded at the standard concentration. Then, a stoichiometric quantity of the competing ion was added, the solution stirred, and a second intensity reading taken. A final reading was taken 3 min after the addition of a stoichiometric quantity of molybdate (or vanadate).

Determination of Relative Quantum Yields. The relative quantum yields were calculated according to eq 1 by using an aerated aqueous solution of [Ru(bpy)$_3$]Cl$_2$ as the standard (ϕ_{std} = 0.028[31]). Φ_{sam} and Φ_{std} are the quantum yields of the sample and the standard, respectively. A_{sam} and A_{std} are the absorbances of the sample (in acetonitrile/water 20:1) and the standard (in water) at the excitation wavelength (λ_{exc} = 400 nm). I_{sam} and I_{std} are the integrated emission intensities obtained from the corrected emission spectra, recorded with aerated solutions at room temperature.

$$\Phi_{sam} = \Phi_{std}\left(\frac{A_{std}}{A_{sam}}\right)\left(\frac{I_{sam}}{I_{std}}\right) \quad (1)$$

Results and Discussion

Synthesis and Characterization of [Ru(bpy)$_2$(H_2-L^3)]-(PF_6)$_2$, 3(PF_6)$_2$, and [ReBr(CO)$_3$(H_2-L^3)], 4. 2,3-Dimethoxy-*N*-(1,10-phenanthroline-5-yl)benzamide, **Me_2-L^3**, was synthesized from commercially available 2,3-dimethoxybenzoic acid and 1,10-phenanthroline-5-yl amine, as shown in Scheme 2. 2,3-Dimethoxybenzoic acid anhydride was formed using DCC[32] (*N*,*N*′-dicyclohexylcarbodiimide) and reacted with 1,10-phenanthroline-5-yl amine. Since 1,10-phenanthroline-5-yl amine was observed to form insoluble decomposition products upon exposure to light, the second step of the reaction was carried out in the dark.

(31) Nakamaru, K. *Bull. Chem. Soc. Jpn.* **1982**, 2697.
(32) Deroo, S.; Defrancq, E.; Moucheron, C.; Mesmaeker, A. K.-D.; Dumy, P. *Tetrahedron Lett.* **2003**, *44*, 8379.

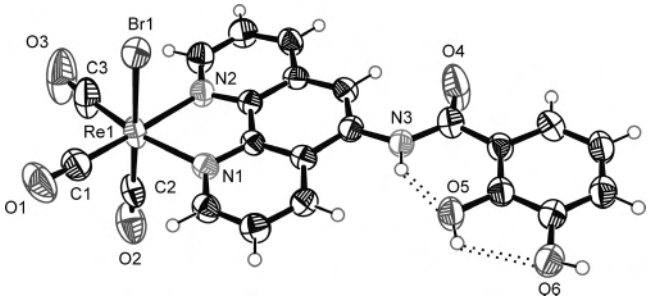

Figure 1. ORTEP plot (50% probability ellipsoids) of the molecular structure of **4**.

Table 1. Selected Bond Distances (Å) and Angles (deg) of **4**·CH_3CN

Re(1)−C(1)	1.920(8)	Re(1)−Br(1)	2.6254(8)
Re(1)−C(2)	1.934(8)	Re(1)−N(1)	2.195(5)
Re(1)−C(3)	1.894(8)	Re(1)−N(2)	2.156(5)
N(3)−O(5)	2.649(7)	O(6)−Br(1)#1[a]	3.317(5)
O(5)−O(6)	2.671(6)	C(16)−O(4)	1.207(8)
O(5)−N(4)	2.823(10)	C(16)−N(3)	1.353(8)
C(1)−Re(1)−C(2)	90.0(3)	C(1)−Re(1)−N(1)	100.1(2)
C(3)−Re(1)−C(1)	91.7(3)	C(2)−Re(1)−N(1)	92.5(2)
C(3)−Re(1)−C(2)	87.3(4)	C(2)−Re(1)−N(2)	97.8(2)
C(1)−Re(1)−Br(1)	86.9(2)	N(1)−Re(1)−Br(1)	86.18(12)
C(2)−Re(1)−Br(1)	176.4(2)	N(2)−Re(1)−Br(1)	85.15(13)
C(3)−Re(1)−Br(1)	94.7(3)	N(2)−Re(1)−N(1)	75.28(18)
C(8)−N(3)−C(16)	128.7(6)	N(3)−C(16)−O(4)	122.7(6)

[a] Symmetry transformation used to generate equivalent atom: #1, $-x$, $-y+1$, $-z+1$.

The complexes $[Ru(bpy)_2(\mathbf{Me_2\text{-}L^3})]^{2+}$ and $[ReBr(CO)_3(\mathbf{Me_2\text{-}L^3})]$ were formed by refluxing the methyl-protected ligand with the respective luminophore precursors, $[Ru(bpy)_2Cl_2]$[33] and $[Re(CO)_5Br]$,[34] according to published procedures.[35,36] The neutral rhenium-based sensor was isolated directly from the reaction mixture while the cationic ruthenium complex was precipitated as the hexafluorophosphate salt. Both complexes were characterized by ^1H and ^{13}C NMR spectroscopy and ESI mass spectrometry. The aromatic region in the spectrum of $[Ru(bpy)_2(\mathbf{Me_2\text{-}L^3})](PF_6)_2$ was assigned based on a $^1H-^1H$ COSY NMR spectrum.

The quantitative demethylation of both complexes was achieved with BBr_3[37] and confirmed by TLC, mass spectrometry, NMR spectroscopy, and X-ray crystallography. In the proton NMR spectra of both compounds, the completeness of the deprotection was verified by the absence of the two characteristic methyl resonances.

Crystal Structure Determinations. The Crystal Structure of $[ReBr(CO)_3(\mathbf{H_2\text{-}L^3})]$. Single crystals of $[ReBr(CO)_3(\mathbf{H_2\text{-}L^3})]$ (**4**) were obtained by the slow evaporation of a concentrated solution of **4** in acetonitrile. The molecular structure of the complex is shown in Figure 1, selected bond angles and distances are given in Table 1 and crystal data are summarized in Table 2. The coordination geometry of the rhenium center is distorted octahedral, as is typical for diimine-coordinated *fac*-$Re^I(CO)_3$ units. The small N(1)−Re−N(2) bond angle of 75.28° is determined by the bite angle of the bidentate phenanthroline ligand. The Re−C and Re−N distances are within the expected range.[38−41]

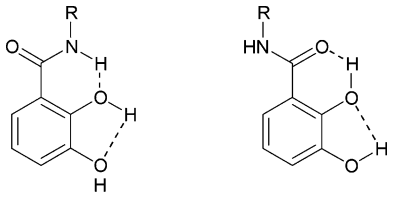

I **II**

Figure 2. Intramolecular hydrogen bonds in 2,3-dihydroxybenzamides.

The conformation of the ligand $\mathbf{H_2\text{-}L^3}$ in **4** is of interest, since it determines the degree of electronic coupling between the metal-binding unit and the signaling unit. In **4**, the dihedral angle between the fitted planes of the catechol and the phenanthroline deviates by only 4.1(2)° from coplanarity. The catecholamide unit is held planar by an intramolecular hydrogen bond formed between the amide N−H and the ortho O atom of the catechol unit ($d_{N(3)-O(5)} = 2.649(7)$ Å). A second intramolecular hydrogen bond is formed between the ortho O−H and the meta O atoms of the catechol ring ($d_{O(5)-O(6)} = 2.671(6)$ Å).

A survey of the Cambridge Structural Database revealed that this hydrogen-bond orientation is unusual for a 2,3-dihydroxybenzamide. In 9 out of the 10 structures reported, it is the carbonyl oxygen of the amide link that interacts with the ortho-hydroxyl group, as shown as **II** in Figure 2. Recent DFT calculations confirm that hydrogen-bond orientation **II** is significantly more stable than orientation **I**.[42]

In the structure of **4**, however, the unusual hydrogen bond orientation **I** allows the formation of an additional intermolecular hydrogen bond between the O−H group in the meta position of the catechol and the bromide of an adjacent rhenium luminophore (Figure 3 and Supporting Information S1). The observed O(6)−Br(1′) distance of 3.317(5) Å is consistent with those described in the literature.[43] In addition, a weak hydrogen bond is formed between the ortho-hydroxyl group and an acetonitrile solvent molecule ($d_{O(5)-N(4)} = 2.823$ Å). Interestingly, the only other structure reported to date to adopt hydrogen-bond orientation **I** also contains additional intermolecular hydrogen-bonding interactions that involve polar solvent molecules.[44] This demonstrates that the presence of intermolecular hydrogen-bond acceptors can change the orientation of the intramolecular hydrogen bonds

(33) Sullivan, B. P.; Salmon, D. J.; Meyer, T. J. *Inorg. Chem.* **1978**, *17*, 3334.
(34) Kutal, C.; Weber, M. A.; Ferraudi, G.; Geiger, D. *Organomet.* **1985**, *4*, 2161.
(35) Sacksteder, L.; Zipp, A. P.; Brown, E. A.; Streich, J.; Demas, J. N.; DeGraff, B. A. *Inorg. Chem.* **1990**, *29*, 4335.
(36) Wu, F.; Riesgo, E.; Pavalova, A.; Kipp, R. A.; Schmehl, R. H.; Thummel, R. P. *Inorg. Chem.* **1999**, *38*, 5620.
(37) O'Brien, L.; Duati, M.; Rau, S.; Guckian, A. L.; Keyes, T. E.; O'Boyle, N. M.; Serr, A.; Görls, H.; Vos, J. G. *Dalton Trans.* **2004**, 514.
(38) Martí, A. A.; Mezei, G.; Maldonado, L.; Paralitici, G.; Raptis, R. G.; Colón, J. L. *Eur. J. Inorg. Chem.* **2005**, 118.
(39) Lazarides, T.; Miller, T. A.; Jeffery, J. C.; Ronson, T. K.; Adams, H.; Ward, M. D. *Dalton Trans.* **2005**, 528.
(40) Yam, V. W.-W.; Chong, S. H.-F; Cheung, K.-K. *Organomet.* **2000**, *19*, 5092.
(41) Busby, M.; Gabrielsson, A.; Matousek, P.; Towrie, M.; Di Bilio, A. J.; Gray, H. B.; Vlček, A., Jr. *Inorg. Chem.* **2004**, *43*, 4994.
(42) Hay, B. P.; Dixon, D. A.; Vargas, R.; Garza, J.; Raymond, K. N. *Inorg. Chem.* **2001**, *40*, 3922.
(43) Depree, C. V.; Ainscough, E. W.; Brodie, A. M.; Gainsford, G. J.; Lensink, C. *Acta Crystallogr.* **2000**, *C56*, 17.
(44) Zimmer, B.; Bulach, V.; Drexler, C.; Erhardt, S.; Hosseini, M. W.; De Cian, A. *New J. Chem.* **2002**, *26*, 43.

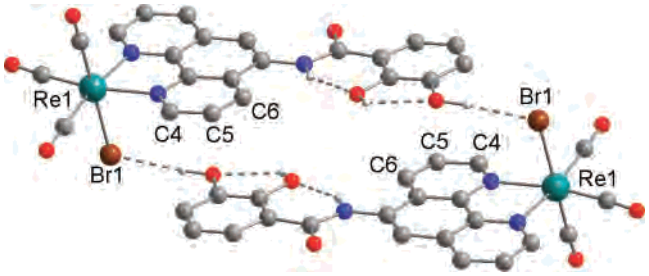

Figure 3. Ball-and-stick representation of two adjacent [ReBr(CO)$_3$(**H$_2$-L^3**)] molecules. O atoms are shown in red, N atoms in blue, and H atoms except NH and OH have been omitted for clarity.

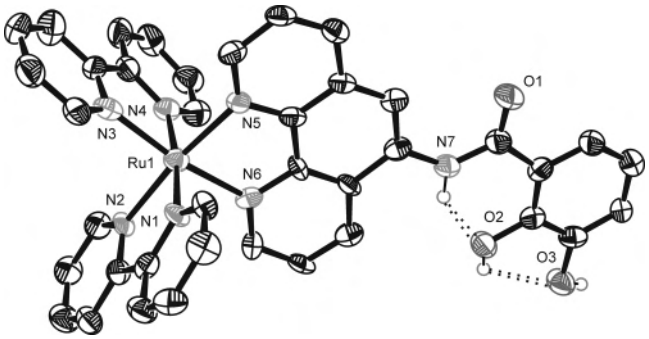

Figure 4. ORTEP plot (50% probability ellipsoids) of the molecular structure of **3** (H atoms, except those of NH and OH, bromide counterions, and lattice water molecules, are not shown).

in 2,3-dihydroxybenzamides in the solid state. The proton NMR data reveal, however, that **4** changes to the usual hydrogen-bond orientation **II** in solution. Upon deprotection, the signal of the amide proton shifts dramatically from 11.10 ppm in [ReBr(CO)$_3$(**Me$_2$-L^3**)] to 6.97 ppm in **4**. This increase in shielding indicates that the amide proton in the latter is not involved in hydrogen bonding.

The two sensor molecules in the unit cell are further held together through $\pi-\pi$-stacking interactions between the **H$_2$-L^3** ligands (Figures 3 and Supporting Information S1). Carbon atom C5 of one of the electron-poor pyridine rings of the phenanthroline is positioned over the center of the π electrons of the electron-rich catechol ring. The intermolecular distance between the center of the catechol ring and C5 of 3.3 Å indicates significant aromatic−aromatic interactions. Parallel-displaced aromatic−aromatic interactions of this type are often observed in π-stacked systems that involve nitrogen-containing heterocycles.[45]

The Crystal Structure of [Ru(bpy)$_2$(H$_{1.51}$-L^3)]Br$_{1.49}$. Attempts to grow crystals of the PF_6 salt of [Ru(bpy)$_2$(**H$_2$-L^3**)]$^{2+}$ (**3**) were unsuccessful. After anion exchange, however, single crystals of the bromide salt could be obtained by slow evaporation of a concentrated solution in aqueous acetonitrile. The structure of the complex is shown in Figure 4, crystal data are summarized in Table 2 and selected bond angles and distances are given in Table 3. The ruthenium-based luminophore has approximately octahedral geometry, as expected for such systems.[46]

(45) Janiak, C. *J. Chem. Soc., Dalton Trans.* **2000**, 3885.
(46) Rillema, D. P.; Jones, D. S.; Levy, H. A. *J. Chem. Soc., Chem. Comm.* **1979**, 849.

Table 2. Crystal Data and Summary of Data Collection and Refinement Details

	[ReBr(CO)$_3$(**H$_2$-L^3**)]·CH$_3$CN	[Ru(bpy)$_2$(**H$_{1.51}$-L^3**)]Br$_{1.49}$·6H$_2$O
empirical formula	$C_{24}H_{16}BrN_4O_6Re$	$C_{39}H_{29}Br_{1.49}N_7O_9Ru$
fw	722.52	959.73
T (K)	298(2)	115(2)
cryst syst	triclinic	monoclinic
space group	$P\bar{1}$	$C2/c$
a (Å)	7.3389(6)	21.159(6)
b (Å)	12.8693(10)	17.582(5)
c (Å)	13.8173(11)	22.842(7)
α (deg)	70.464(2)	90
β (deg)	86.758(2)	98.204(7)
γ (deg)	76.554(2)	90
V (Å^3)	1195.84(17)	8411(4)
Z	2	8
ρ_{calcd} (mg/m^3)	2.007	1.516
μ (mm^{-1})	6.800	1.848
F(000)	692	3840.9
θ range (deg)	1.56−25.10	1.69−19.04
index ranges	$-8 \le h \le 8$ $-15 \le k \le 14$ $-16 \le l \le 12$	$-19 \le h \le 19$ $-12 \le k \le 16$ $-20 \le l \le 20$
reflns collected	6780	12 308
independent reflns	4202 [R(int) = 0.0281]	3416 [R(int) = 0.0498]
data/restraints/params	4202/0/327	3416/0/543
GOF on F^2	1.023	1.055
R indices [$I > 2\sigma(I)$]	$R_1 = 0.0356$, $R_2 = 0.0799$	$R_1 = 0.0483$, $R_2 = 0.1230$
R indices (all data)	$R_1 = 0.0503$, $R_2 = 0.0855$	$R_1 = 0.0677$, $R_2 = 0.1349$
largest diff peak/hole (e Å^{-3})	1.972/−0.585	1.171/−0.437

Table 3. Selected Bond Distances (Å) and Angles (deg) of [Ru(bpy)$_2$(**H$_{1.51}$-L^3**)]Br$_{1.49}$·6H$_2$O

Ru(1)−N(1)	2.048(7)	Ru(1)−N(4)	2.060(7)
Ru(1)−N(2)	2.051(6)	Ru(1)−N(5)	2.065(7)
Ru(1)−N(3)	2.045(7)	Ru(1)−N(6)	2.058(6)
N(7)−O(2)	2.641(9)	O(3)−Br(2)#2[a]	3.071(6)
O(2)−O(3)	2.654(8)	C(33)−N(7)	1.358(11)
O(2)−Br(1)#1[a]	3.063(7)	C(33)−O(1)	1.225(10)
N(3)−Ru(1)−N(1)	96.8(3)	N(2)−Ru(1)−N(4)	97.4(3)
N(3)−Ru(1)−N(2)	92.7(2)	N(2)−Ru(1)−N(4)	97.4(3)
N(1)−Ru(1)−N(2)	78.6(3)	N(6)−Ru(1)−N(4)	94.6(3)
N(1)−Ru(1)−N(6)	90.1(2)	N(3)−Ru(1)−N(5)	93.7(3)
N(2)−Ru(1)−N(6)	94.7(3)	N(6)−Ru(1)−N(5)	79.3(3)
N(3)−Ru(1)−N(4)	79.0(3)	N(4)−Ru(1)−N(5)	87.9(3)
C(33)−N(7)−C(32)	129.6(8)	N(7)−C(33)−O(1)	121.8(9)

[a] Symmetry transformations used to generate equivalent atoms: #1, $-x+1, -y+2, -z+1$; #2, $x, y+1, z-1$.

The conformation of **H$_2$-L^3** in **3** is very similar to the one observed in **4**. Again, the ligand is nearly planar. The dihedral angle between the fitted planes of the catechol and the phenanthroline refined to 4.8(4)°. Intramolecular hydrogen bonds are formed between the amide N−H and the ortho O atoms of the catechol ($d_{N(7)-O(2)} = 2.641(9)$ Å) and the ortho O−H and the meta O atoms of the catechol ring ($d_{O(5)-O(6)} = 2.654(8)$ Å), again corresponding to orientation **I** in Figure 2. This orientation appears to be favored in this case through additional intermolecular interactions between theO−H groups of the catechol with the bromide counterions ($d_{O(2)-Br(1')} = 3.317(5)$ Å and $d_{O(3)-Br(2'')} = 3.317(5)$ Å).

The bromide counterions in the structure are disordered over four sites, one of which lies on a special position. The

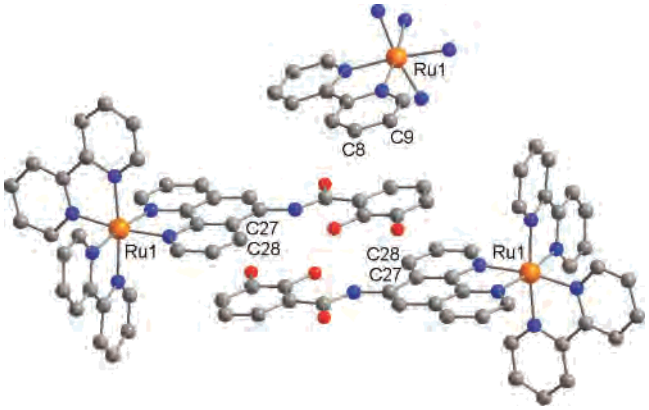

Figure 5. Ball-and-stick representation of two selected $[Ru(bpy)_2(\mathbf{H_2}\text{-}\mathbf{L^3})]^{2+}$ complexes and of the Ru−bpy fragment of an adjacent complex, illustrating aromatic−aromatic interactions. O atoms are shown in red, N atoms in blue, and H atoms have been omitted for clarity.

occupancy of the bromides was refined and gave a total of 1.49 bromides per asymmetric unit. Attempts to restrain the total number of bromide ions in the asymmetric unit to two, in order to balance the 2+ charge of the ruthenium, resulted in a significant increase in the *R* value. Since the crystals were obtained from a solution at pH 4.5, which is close to the pK_a value of the 2-hydroxy-group (vide infra), approximately half of the catechol units are likely to be deprotonated, giving rise to an empirical formula of $[Ru(bpy)_2(\mathbf{H_{1.51}}\text{-}\mathbf{L^3})]Br_{1.49}$. Although the data were collected at low temperature to increase the resolution of the structure, the positions of the hydrogen atoms could not be located in the Fourier difference map. The hydrogen atoms of the $[Ru(bpy)_2(\mathbf{H_2}\text{-}\mathbf{L^3})]^{2+}$ component were thus calculated using a riding model.

The structure revealed that $\mathbf{H_2}\text{-}\mathbf{L^3}$ is again involved in intermolecular $\pi-\pi$-stacking interactions. Its catechol ring is sandwiched between the phenanthroline unit and a bipyridine ligand of the adjacent $[Ru(bpy)_2(\mathbf{H_2}\text{-}\mathbf{L^3})]^{2+}$ complexes (Figures 5 and Supporting Information S2). The intermolecular distance between the centroid of the catechol ring and the closest atom of the bipyridine ligand (C9) at 3.35 Å is very similar to the distance of 3.4 Å between the centroid and the closest atom of the phenanthroline system (C27) .

In summary, the crystal structures of **3** and **4** reveal that the conformation of $\mathbf{H_2}\text{-}\mathbf{L^3}$ in the solid state does not change significantly on moving from a $[ReBr(CO)_3(phen)]$- to a $[Ru(bpy)_2(phen)]^{2+}$-type luminophore. The catechol and phenanthroline rings are essentially coplanar in both structures and allow π-overlap and electronic coupling between the metal-binding units and the luminophores.

Electronic Absorption and Emission Properties of $[Ru(bpy)_2(\mathbf{H_2}\text{-}\mathbf{L^3})](PF_6)_2$, $\mathbf{3}(PF_6)_2$. The electronic absorption and emission properties of $[Ru(bpy)_2(\mathbf{Me_2}\text{-}\mathbf{L^3})](PF_6)_2$ and $[Ru(bpy)_2(\mathbf{H_2}\text{-}\mathbf{L^3})](PF_6)_2$ were investigated between pH 0.1 and 10. Due to the limited water solubility of the hexafluorophosphate salts, a mixed solvent system consisting of acetonitrile and water (20:1) was used. Adjustments to the pH were carried out with a 0.6 M solution of HCl in this solvent system and a 0.6 M solution of tetramethyl ammonium hydroxide in water.

Table 4. Selected Spectroscopic Data for $[Ru(bpy)_2(\mathbf{Me_2}\text{-}\mathbf{L^3})](PF_6)_2$ and $[ReCl(CO)_3(\mathbf{Me_2}\text{-}\mathbf{L^3})]$ (Aerated Solutions at Room Temperature, Solvent acetonitrile/water in ratio of 20:1)

compound	absorption λ_{abs}/nm (10^{-3} ϵ/ M^{-1} cm^{-1})	emission λ_{max}/nm	quantum yield Φ_{em}[b]
$[Ru(bpy)_2(\mathbf{Me_2}\text{-}\mathbf{L^3})](PF_6)_2$	400 (7.46), 450 (16.50)	625	0.011
$[ReCl(CO)_3(\mathbf{Me_2}\text{-}\mathbf{L^3})]$[a]	390 (4.00), 400 (3.68)	635	0.004

[a] $[ReCl(CO)_3(\mathbf{Me_2}\text{-}\mathbf{L^3})]$ was synthesized to allow a direct comparison with the reported spectroscopic data of $[ReCl(CO)_3(phen)]$-type complexes.[53−55] [b] Relative luminescence quantum yield determined by using $[Ru(bpy)_3]Cl_2$ as the standard ($\Phi = 0.028$), $\lambda_{exc} = 400$ nm.

The spectroscopic properties of the methyl-protected derivative $[Ru(bpy)_2(\mathbf{Me_2}\text{-}\mathbf{L^3})](PF_6)_2$ are summarized in Table 4. They agree well with the properties reported for similar $[Ru(bpy)_2(phen)]^{2+}$-type complexes.[26,47] While the absorption and emission spectra of $[Ru(bpy)_2(\mathbf{Me_2}\text{-}\mathbf{L^3})](PF_6)_2$ (Supporting Information, Figure S3) are pH-independent, the absorption spectrum of $[Ru(bpy)_2(\mathbf{H_2}\text{-}\mathbf{L^3})](PF_6)_2$, $\mathbf{3}(PF_6)_2$, changes with pH, as shown in Figure 6. By comparison with the reported spectrum of $[Ru(bpy)_3]^{2+}$ and the spectra of related polypyridine complexes,[48] the lowest energy band in the absorption spectra can be assigned to a Ru(dπ) → bpy or phen(π*) charge transfer (metal-to-ligand charge-transfer, MLCT) transition. While the MLCT absorbance at around 450 nm shows only little pH dependence in $\mathbf{3}(PF_6)_2$, the ligand-based absorbance at 365 nm increases significantly with pH. With reference to the pH dependence of the absorption spectra of 2,3-dihydroxybenzamides, which generally show an increase in absorbance upon deprotonation of the OH group in the 2-position,[49] this increase can be attributed to the formation of $[Ru(bpy)_2(\mathbf{H}\text{-}\mathbf{L^3})]^+$. From the inflection point, a pK_a value of approximately 4.5 can be estimated. This pK_a value is comparatively low for a 2,3-dihydroxybenzamide[50] due to the electron-withdrawing effect of the electron-deficient phenanthroline unit that is enhanced by the coordinated positively charged luminophore.

Upon excitation into the MLCT band at $\lambda_{max} = 450$ nm, acidic solutions of $\mathbf{3}(PF_6)_2$ in air-equilibrated aqueous acetonitrile at room temperature show an intense emission from the corresponding ^{3}MLCT state with a λ_{max} of 610 nm (Figure 7). The intensity of the emission decreases sigmoidally with increasing pH. The inflection point is located at pH 4.4. For similar ruthenium complexes, it was shown that the inflection point of the emission titration (pH_i) can be related to the excited-state pK_a* via eq 2, where τ_{HS} and τ_{S^-} are the lifetimes of the protonated and deprotonated species,

(47) Li, M.-J.; Chu, W.-K.; Zhu, N.; Yam, V. W.-W. *Inorg. Chem.* **2007**, *46*, 720.
(48) Juris, A; Balzani, V.; Barigelletti, F.; Campagne, S.; Belser, P.; von Zelewsky, A. *Coord. Chem. Rev.* **1988**, *84*, 85.
(49) (a) Garett, T. M.; McMurry, T. J.; Hosseini, M. W.; Reyes, Z. E.; Hahn, F. E.; Raymond, K. N. *J. Am. Chem. Soc.* **1991**, *113*, 2965. (b) Cohen, S. M.; Meyer, M.; Raymond, K. N. *J. Am. Chem. Soc.* **1998**, *120*, 6277.
(50) Raymond, K. N.; Mueller, G.; Matzanke, B. F. *Top. Curr. Chem.* **1984**, *123*, 49.

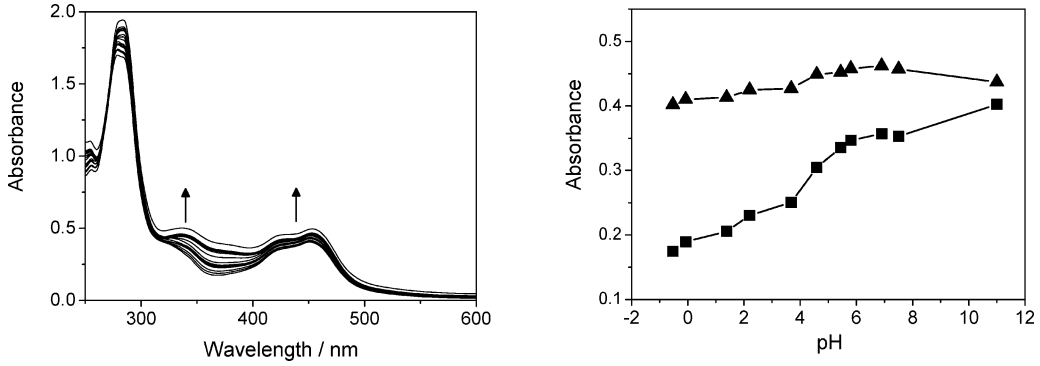

Figure 6. Left: Absorption spectra recorded during the titration of an acidic solution (0.02 mM) of $[Ru(bpy)_2(\mathbf{H_2\text{-}L^3})](PF_6)_2$ in aqueous acetonitrile with an aqueous tetramethylammonium hydroxide solution. The baseline rises at pH 12 since the added quaternary ammonium salt makes acetonitrile and water less miscible. Right: Plot of the absorbance at 365 nm (■) and 450 nm (▲) as a function of pH.

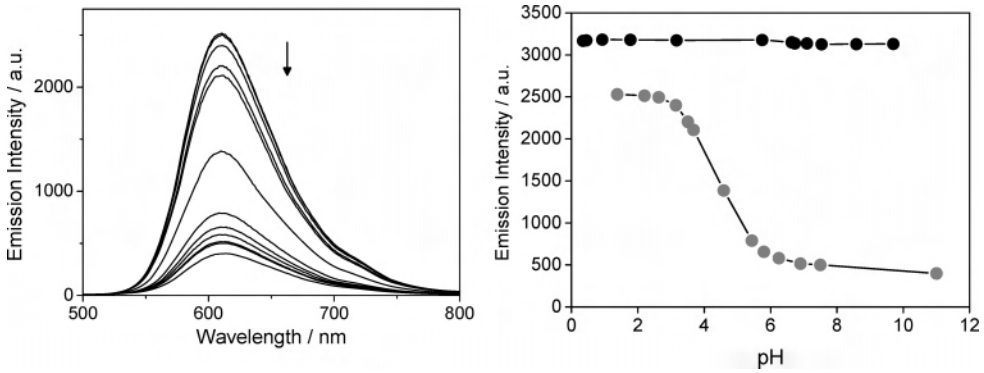

Figure 7. Left: Emission spectra (uncorrected, $\lambda_{exc} = 450$ nm) recorded during the titration of an acidic 0.02 mM solution of $[Ru(bpy)_2(\mathbf{H_2\text{-}L^3})](PF_6)_2$ in aqueous acetonitrile with an aqueous tetramethylammonium hydroxide solution. Right: Emission intensity at maximum (610 nm) versus pH for $[Ru(bpy)_2(\mathbf{H_2\text{-}L^3})](PF_6)_2$ (gray circles) and $[Ru(bpy)_2(\mathbf{Me_2\text{-}L^3})](PF_6)_2$ (black circles).

respectively.[51] We have determined the lifetimes of the protonated and deprotonated form of **3** from time-resolved absorption and emission data and will report the results and the pK_a* of **3** in a follow-up paper. Since the inflection point pH_i, however, is similar to the ground-state pK_a value of the 2-hydroxy-group, it can already be concluded here that the intensity decrease is caused by the deprotonation of the catechol unit. This assertion is further supported by the observation that the emission intensity of the protected sensor derivative $[Ru(bpy)_2(\mathbf{Me_2\text{-}L^3})](PF_6)_2$ is pH-independent (Figure 7). In addition, emission quenching upon deprotonation of appended phenolic OH groups was reported for similar systems.[52,53]

$$pK_a^* = pH_i + \log \tau_{HS}/\tau_{S^-} \qquad (2)$$

The ~20% drop in emission intensity upon deprotection of $[Ru(bpy)_2(\mathbf{Me_2\text{-}L^3})]^{2+}$ can be attributed to interactions of the free catechol unit with the solvent. Since the hydroxyl groups form hydrogen bonds with acetonitrile and water, the number of nonradiative decay pathways increases and the emission intensity is reduced.

Electronic Absorption and Emission Properties of $[ReBr(CO)_3(\mathbf{H_2\text{-}L^3})]$, 4. The spectroscopic properties of the methyl-protected derivative $[ReCl(CO)_3(\mathbf{Me_2\text{-}L^3})]$ are summarized in Table 4. They agree well with the properties reported for similar $[ReCl(CO)_3(diimine)]$ complexes.[53−55] The absorption and emission spectra of $[ReCl(CO)_3(\mathbf{Me_2\text{-}L^3})]$ (Supporting Information, Figure S4) and $[ReBr(CO)_3(\mathbf{Me_2\text{-}L^3})]$ are similar and independent of the pH of the solution. In contrast, the titration of an acidic solution of **4** with base revealed a significant pH dependence (Figure 8), indicating that the MLCT transition with $\lambda_{max} = 395$ nm overlaps with pH-dependent ligand-based transitions. This is not unusual; the Re(dπ) → phen(π*) charge-transfer transitions in rhenium(I) tricarbonyl complexes are often found very close to the low-energy side of intense ligand-based $\pi \rightarrow \pi^*$ absorption bands.[24,52] In **4**, the addition of base leads to an increase in the absorbance at 390 nm, which is again due to the deprotonation of the ortho-OH group of the catecholamide unit. In this case, $[ReBr(CO)_3(\mathbf{H\text{-}L^3})]^-$ is formed. A sigmoidal fit of the corresponding pH profile gives a midpoint value of 5.75 ± 0.05, which is significantly higher than the estimated midpoint value of 4.5 for $[Ru(bpy)_2(\mathbf{H_2\text{-}L^3})]^{2+}$. This difference can be attributed to the fact that the cationic Ru^{II} complex can stabilize the negative charge resulting from the deprotonation more effectively than the Re^{I}-based sensor. Similar differences in pK_a values have been observed for 1,10-phenanthroline-5-carboxylic acid when coordinated to related Ru^{II}- and Re^{I}-containing chromophores.[27]

(51) Vos, J. G. *Polyhedron* **1992**, *11*, 2285.
(52) Burdinski, D.; Bothe, E.; Wieghardt, K. *Inorg. Chem.* **2000**, *39*, 105.
(53) Reece, S. Y.; Nocera, D. G. *J. Am. Chem. Soc.* **2005**, *127*, 9448.
(54) Kalyanasundaram, K. *Photochemistry of Polypyridine and Porphyrin Complexes*; Academic Press: London, 1992; Chapter 10.
(55) Wrighton, M.; Morse, D. L. *J. Am. Chem. Soc.* **1974**, *96*, 998.

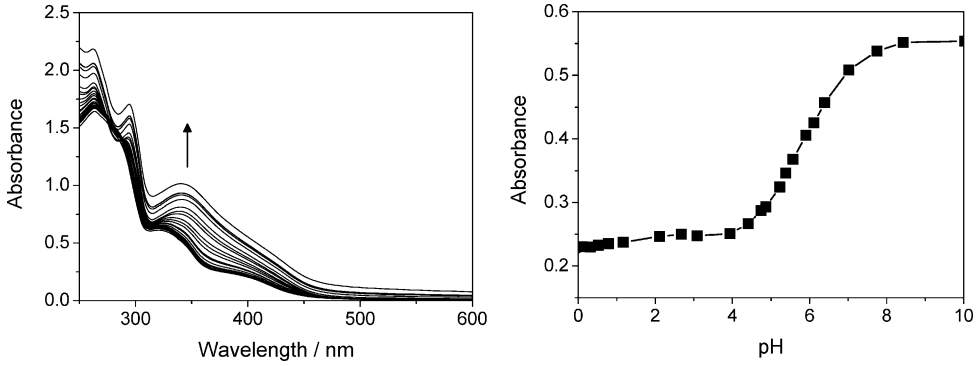

Figure 8. Left: Absorption spectra recorded during the titration of an acidic solution (0.1 mM) of [ReBr(CO)$_3$(**H$_2$-L^3**)] in aqueous acetonitrile with an aqueous tetramethylammonium hydroxide solution. The baseline rises at high pH since the added quaternary ammonium salt makes acetonitrile and water less miscible. Right: Plot of the absorbance at 390 nm as a function of pH.

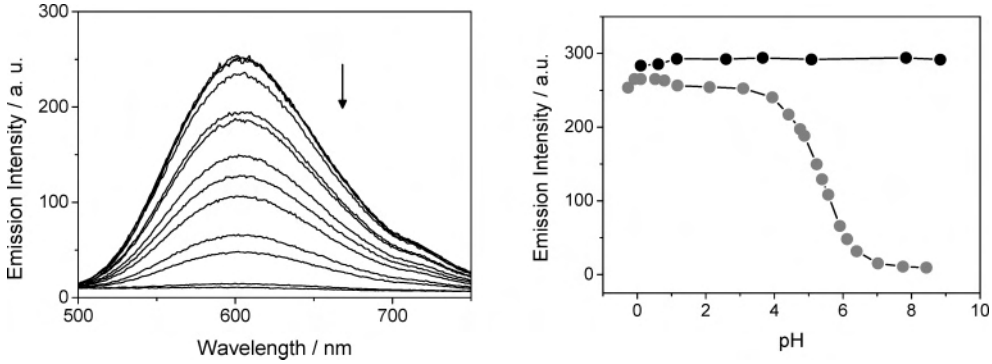

Figure 9. Left: Selected emission spectra (uncorrected, λ_{exc} = 390 nm) recorded during the titration of an acidic 0.1 mM solution of [ReBr(CO)$_3$(**H$_2$-L^3**)] in aqueous acetonitrile with an aqueous tetramethylammonium hydroxide solution. Right: Emission intensity at maximum (605 nm) versus pH for [ReBr(CO)$_3$(**H$_2$-L^3**)] (gray circles) and [ReBr(CO)$_3$(**Me$_2$-L^3**)] (black circles).

Acidic solutions of **4** in aqueous acetonitrile emit with a λ_{max} at 605 nm when excited at 390 nm. The emission spectrum of the acidic solution resembles that of the methyl-protected complex [ReBr(CO)$_3$(**Me$_2$-L^3**)]; however, the intensity of the emission of **4** decreases upon the addition of base (Figure 9). At pH 10, only ca. 5% of the initial emission intensity is observed. This decrease can again be ascribed to the deprotonation of the ortho-OH group. The midpoint of the pH-response was fitted to a value of 5.35 ± 0.05. As expected, the emission intensity of the methyl-protected sensor [ReBr(CO)$_3$(**Me$_2$-L^3**)] remains constant between pH 0.1 and 10.

Oxometalate Detection. pH-Profiles. The addition of 0.5 equiv of molybdate, tungstate, or vanadate to solutions of **4** results in a decrease of the emission intensity in the acidic pH-range (Figures 10 and 11). Consequently, **4** can be used as a chemosensor for these species. The decrease in emission intensity in the presence of the oxometalates can be attributed to the deprotonation of the catechol units upon metal-ion coordination. The observation that the emission intensity of the methyl-protected derivative [ReBr(CO)$_3$(**Me$_2$-L^3**)] is not influenced by the presence of molybdate supports this assertion and demonstrates that the decrease in emission intensity is not due to intermolecular quenching processes.

Molybdate and tungstate as well as vanadate tend to condense in concentrated acidic solutions to form polyoxometalates. Since the 0.05 mM oxometalate concentrations used in the study with **4** are comparatively high, we were interested in investigating whether polyoxometalate formation would be indicated by **4**. For this purpose, the pH profiles were recorded again after pre-acidification of the solutions to pH 1. It emerged that the pH profile of **4** in the presence of tungstate shows only a very slight deviation from the profile of the free **4** upon titration of the pre-acidified solution with base. The two combined pH profiles obtained in the presence of tungstate thus displayed a pronounced hysteresis loop (Figure 11). A subsequent investigation of the reversibility of the titrations with molybdate and vanadate revealed that these also show some degree of hysteresis (Supporting Information, Figure S5). This behavior is consistent with polyoxometalate formation in the pre-acidified solutions since in the condensed species, the actual concentration of reactive

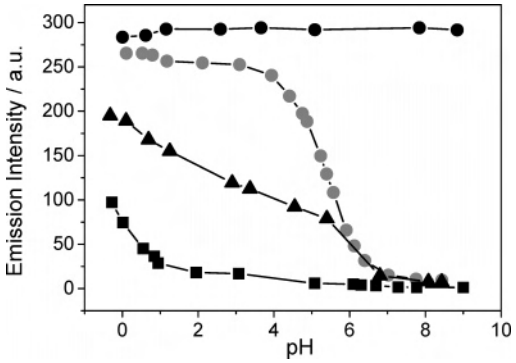

Figure 10. Emission intensity at maximum (605 nm) versus pH for **4** (gray circles), **4** + 0.5 equiv molybdate (black squares), **4** + 0.5 equiv vanadate (black triangles), and [ReBr(CO)$_3$(**Me$_2$-L^3**)] + 0.5 equiv molybdate (black circles) (0.1 mM solutions in aqueous acetonitrile).

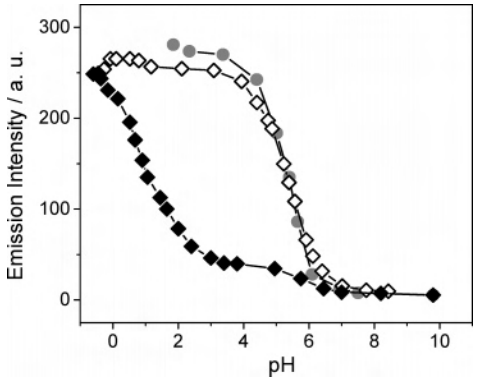

Figure 11. pH profile of [ReBr(CO)$_3$(**H$_2$-L^3**)] (0.1 mM in aqueous acetonitrile) in the presence of 0.5 equiv of tungstate obtained upon titration from low-to-high pH (hollow diamonds) and high-to-low pH (black diamonds) in comparison with the pH profile of [ReBr(CO)$_3$(**H$_2$-L^3**)](gray circles).

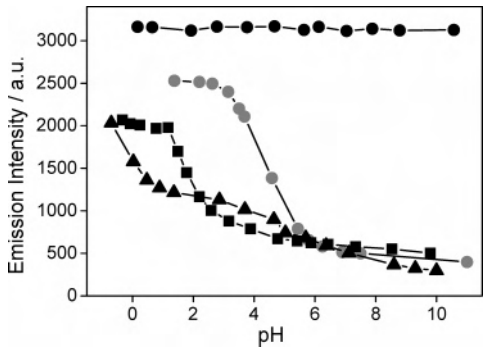

Figure 12. Emission intensity at maximum (610 nm) versus pH for **3** (gray circles), **3** + 0.5 equiv molybdate (black squares), **3** + 0.5 equiv vanadate (black triangles), and [Ru(bpy)$_2$(**Me$_2$-L^3**)]$^{2+}$ + 0.5 equiv molybdate (black circles) (0.02 mM solutions in aqueous acetonitrile).

metal ions that are able to bind to the sensor molecules is reduced and less quenching is observed. The effect is most pronounced for tungstate since polyoxotungstates are particularly inert.[56] Pre-acidification of the analyte solutions to pH 1 could therefore be used for the differentiation of molybdate and tungstate.

Analogous titrations were performed with **3**. As evident from Figure 12, **3** also functions as a chemosensor for molybdate and vanadate in slightly acidic solutions. In the case of **3**, the pre-acidification of the solutions to pH 1 did not have a significant impact on the pH profiles obtained in the presence of molybdate or vanadate (Supporting Information, Figure S6). Since the 0.01 mM concentration at which the reversibility study with [Ru(bpy)$_2$(**H$_2$-L^3**)]$^{2+}$ was carried out is much lower than in the study with [ReBr(CO)$_3$(**Me$_2$-L^3**)], polyoxometalate species are less likely to be prevalent and hysteresis is thus not observed.

In the presence of tungstate, the titration from acidic to basic pH begins essentially as that for the reference complex [Ru(bpy)$_2$(**H$_2$-L^3**)]$^{2+}$. Once the pH level of 5 is reached, however, the decrease in emission intensity levels off and a residual emission intensity of over 50% remains even at the level of pH 12. No other changes to the emission spectra are observed (Figure 13). Upon titration from basic to acidic pH, the emission intensity already starts to increase at ca. pH 7. The reasons for this behavior, which is unusual but reproducible, are still under investigation. Irrespective of the direction of the titration, however, tungstate does not quench the emission significantly below pH 3.5. Consequently, the presence of tungstate does not interfere with the sensing of molybdate or vanadate by **3**.

Selectivity Studies. The selectivity of [Ru(bpy)$_2$(**H$_2$-L^3**)]$^{2+}$ and [ReBr(CO)$_3$(**H$_2$-L^3**)] was investigated by repeating the titrations in the presence of potentially interfering ions. The pH profiles obtained in the presence of biologically relevant metal cations, such as Mn(II), Fe(III), Co(II), Ni(II), and Zn(II) are very similar to the pH profiles of the free sensors (Supporting Information, Figures S5 and S6). Since [Ru(bpy)$_2$(**H$_2$-L^3**)]$^{2+}$ and [ReBr(CO)$_3$(**H$_2$-L^3**)] emit only in the protonated state, cation binding has to take place in acidic media for this interaction to be signaled by emission quenching. The coordination of cations by catechols, however, liberates protons and is thus disfavored at low pH (Scheme 1).

The emission intensities in the presence of Cu(II) at acidic pH values are slightly lowered; however, this decrease is unlikely to be due to the binding of Cu(II) to the catecholamide-based receptor units, since the overall shape of the pH profiles is not changed significantly. Instead the drop can be interpreted as intermolecular quenching based on the observation that under similar conditions the MLCT excited state of the parent complex [Ru(bpy)$_2$(phen)](PF$_6$)$_2$ is quenched to 88% in the presence of an equimolar amount of Cu(PF$_6$)$_2$.[57]

The presence of oxoanions, such as sulfate or phosphate, does not significantly change the pH profiles from that obtained for the free sensor (Supporting Information, Figures S7 and S8). This lack of interference is especially advantageous in biological applications, where high concentrations of these ions can be present. The sensor has also been investigated in the presence of perrhenate, related diagonally in the periodic table to molybdate, but no binding is observed.

Composition of Complexes and Detection Limits. To determine the composition of the Mo and V complexes formed, solutions of [Ru(bpy)$_2$(**H$_2$-L^3**)](PF$_6$)$_2$ and [ReBr(CO)$_3$(**H$_2$-L^3**)] were titrated with aqueous solutions of molybdate and vanadate (Figures 14 and 15). During the titrations, the solutions were buffered at pH values where the difference between the emission intensity of the free and the bound sensors is most pronounced: pH 3 for [Ru(bpy)$_2$(**H$_2$-L^3**)](PF$_6$)$_2$ and pH 4 for [ReBr(CO)$_3$(**H$_2$-L^3**)]. The optimum working pH of the latter is higher since the ortho-OH group in [ReBr(CO)$_3$(**H$_2$-L^3**)] is less acidic.

Upon the addition of molybdate, the emission intensity of both sensors decreases almost linearly until a ratio of sensor-to-molybdate of approximately 2:1 is reached. This ratio is consistent with the predominant formation of *cis*-dioxo-Mo^{VI}−dicatecholate complexes at these pH values. Complexes of this composition are well-documented in the

(56) Tytko, K. H.; Glemser, O. *Adv. Inorg. Chem. Radiochem.* **1976**, *19*, 239.

(57) Riklin, M.; Tran, D.; Bu, X.; Laverman, L. E.; Ford, P. C. *J. Chem. Soc., Dalton Trans.* **2001**, 1813.

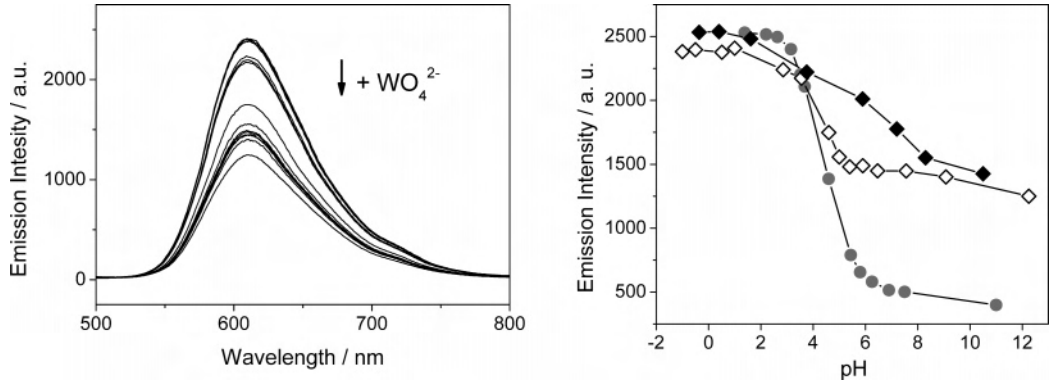

Figure 13. Left: Emission spectra (uncorrected, $\lambda_{exc} = 450$ nm) recorded during the titration of an acidic solution of $[Ru(bpy)_2(\mathbf{H_2}\text{-}\mathbf{L^3})](PF_6)_2$ (0.02 mM) and sodium tungstate (0.01 mM) in aqueous acetonitrile with an aqueous tetramethylammonium hydroxide solution. Right: pH profile of $[Ru(bpy)_2(\mathbf{H_2}\text{-}\mathbf{L^3})](PF_6)_2$ in the presence of 0.5 equiv of tungstate obtained upon titration from low-to-high pH (hollow diamonds) and high-to-low pH (black diamonds) in comparison with the pH profile of $[Ru(bpy)_2(\mathbf{H_2}\text{-}\mathbf{L^3})](PF_6)_2$ (gray circles).

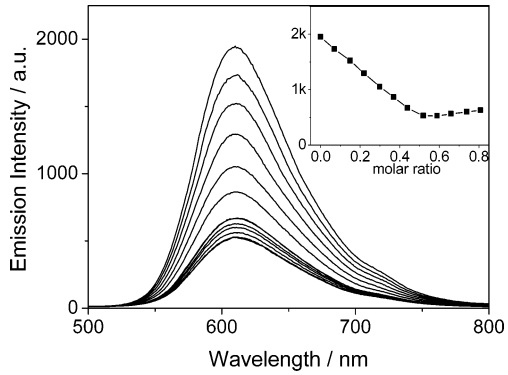

Figure 14. Emission spectra of $[Ru(bpy)_2(\mathbf{H_2}\text{-}\mathbf{L^3})](PF_6)_2$ (0.02 mM) in aqueous acetonitrile in the presence of increasing molybdate concentrations (in aqueous acetonitrile at pH 3.0, buffer 2,6-lutidine, $\lambda_{exc} = 450$ nm). The inset shows the emission intensity at 610 nm as a function of molar MoO_4^{2-} fractions.

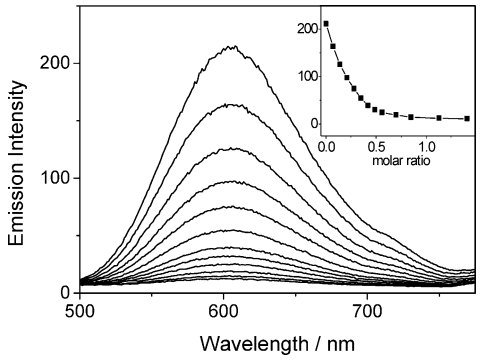

Figure 15. Emission spectra of $[ReBr(CO)_3(\mathbf{H_2}\text{-}\mathbf{L^3})]$ (0.1 mM) in the presence of increasing molybdate concentrations (in aqueous acetonitrile at pH 3.0, buffer 2,6-lutidine, $\lambda_{exc} = 390$ nm). The inset shows the emission intensity at 605 nm as a function of the molar MoO_4^{2-} fractions.

literature.[58,59] Molybdenum binding reduces the ^{3}MLCT emission of $[ReBr(CO)_3(\mathbf{H_2}\text{-}\mathbf{L^3})]$ by ca. 95%, while the emission of $[Ru(bpy)_2(\mathbf{H_2}\text{-}\mathbf{L^3})](PF_6)_2$ decreases by approximately 75%.

Analoguous titrations were carried out with **3** and **4** in the presence of vanadate and also with **4** in the presence of tungstate. The titration curves obtained show similar trends (Supporting Information, Figures S9 and S10).

Table 5. Detection Limits for Molybdate

	sensor	
	$[Ru(bpy)_2(\mathbf{H_2}\text{-}\mathbf{L^3})]^{2+}$, pH 3	$[ReBr(CO)_3(\mathbf{H_2}\text{-}\mathbf{L^3})]$, pH 4
linear range/mol L^{-1}	$0-1.0 \times 10^{-5}$	$0-3.2 \times 10^{-5}$
correlation coeff R^2	0.9982	0.9906
slope m/mol L^{-1} a.u.$^{-1}$	1.4×10^8	4.3×10^6
standard deviation of the blank, s_b/a.u.	8.31	1.87
detection limit		
/mol L^{-1} MoO_4^{2-}	1.8×10^{-7}	1.3×10^{-6}
/μg L^{-1} MoO_4^{2-}	43	315
/μg L^{-1} Mo	17	125

Table 6. Detection Limits for Vanadate

	sensor	
	$[Ru(bpy)_2(\mathbf{H_2}\text{-}\mathbf{L^3})]^{2+}$, pH 3	$[ReBr(CO)_3(\mathbf{H_2}\text{-}\mathbf{L^3})]$, pH 4
linear range/mol L^{-1}	$0-5.0 \times 10^{-6}$	$0-3.4 \times 10^{-5}$
correlation coeff R^2	0.9977	0.9898
slope m/mol L^{-1} a.u.$^{-1}$	1.2×10^8	4.9×10^6
standard deviation of the blank, s_b/a.u.	8.31	1.87
detection limit		
/mol L^{-1} VO_4^{3-}	2.0×10^{-7}	1.1×10^{-6}
/μg L^{-1} VO_4^{3-}	24	132
/μg L^{-1} V	10	58

The detection limits were determined from the linear part of the titration curves according to eq 3,[60] where s_b is the standard deviation of the blank and m is the calibration sensitivity, which corresponds to the slope of the linear part of the calibration curve. The standard deviation of the blank signal was determined from a series of 10 measurements of the emission intensity of the sensor solution in the absenceof oxometalates. The results are summarized in Tables 5 and 6.

$$\text{Detection limit} = 3s_b/m \qquad (3)$$

(58) Griffith, W. P.; Nogueira, H. I. S.; Parkin, B. C.; Sheppard, R. N.; White, A. J. P.; Williams, D. J. J. *J. Chem. Soc., Dalton Trans.* **1995**, 1775.

(59) Duhme, A.-K. *J. Chem. Soc., Dalton Trans.* **1997**, 773.

(60) Skoog, D. A.; West, D. M.; Holler, F. J.; Crouch, S. R. *Fundamentals of Analytical Chemistry*, 8th ed.; Thomson Brooks/Cole: Belmont, 2004; Chapters 6 and 8.

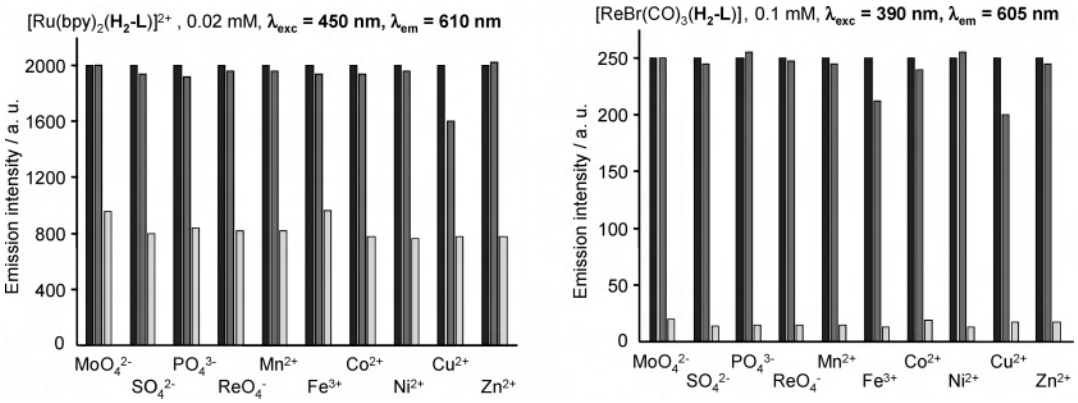

Figure 16. Emission intensity of the indicated sensor (black), the sensor in the presence of a potentially competing ion (dark gray), and the sensor in the presence of the competing ion and molybdate (light gray).

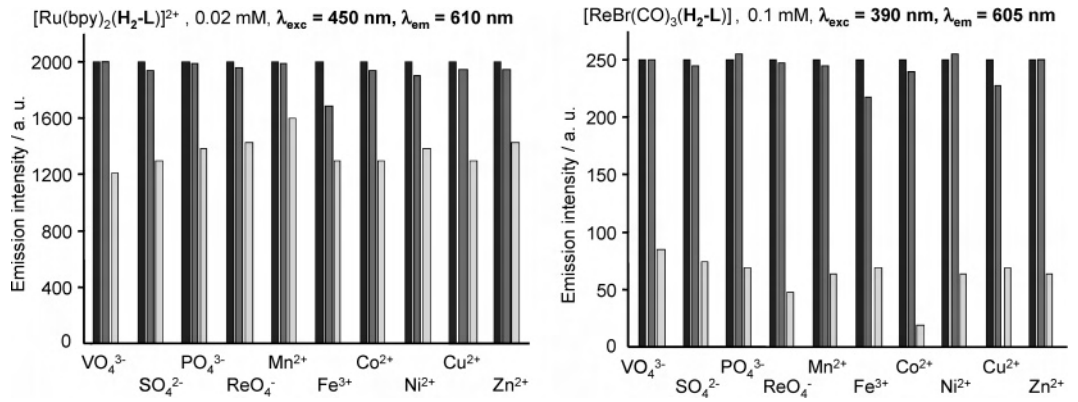

Figure 17. Emission intensity of the indicated sensor (black), the sensor in the presence of a potentially competing ion (dark gray), and the sensor in the presence of the competing ion and vanadate (light gray).

As is evident from Tables 5 and 6, the Ru-based sensor is generally more sensitive than the Re-based sensor. The lower detection limits for molybdate and vanadate in the case of $[Ru(bpy)_2(\mathbf{H_2\text{-}L^3})]^{2+}$ are a consequence of the steeper gradients of the calibration curves, which are caused by the much higher initial emission intensity of the Ru-based luminophore. Although the Ru-based sensor shows a higher residual emission intensity in the presence of molybdate and vanadate than the Re-based sensor, its far stronger emission in the absence of molybdate or vanadate results in a higher calibration sensitivity and lower detection limits.

The fact that the colorimetric determination of molybdate concentrations with catechol has a detection limit of 11 mg L^{-1} [61] shows that the attachment of the catechol receptor unit to Ru- or Re-based luminophores has improved the sensitivity of the method dramatically. The detection limits achieved with $[Ru(bpy)_2(\mathbf{H_2\text{-}L^3})]^{2+}$ and $[ReBr(CO)_3(\mathbf{H_2\text{-}L^3})]$ reach those reported for organic fluorescent reagents. Reported detection limits range from 100 μg L^{-1} of Mo reported for Alizarin red S[62] or 10 μg L^{-1} of Mo at pH 3.0−3.7 for bathophenanthrolinedisulfonate[63] to 0.08 μg L^{-1} of Mo at pH 9.2 for 2-hydroxy-1-naphthaldehydene-8-aminoquinoline.[64] For vanadate, detection limits range from 190 μg L^{-1} of V for the extractive colorimetric detection with 6-chloro-3-hydroxy-7-methyl-2-(2-thienyl)-4*H*-chromen-4-one[65] or the use of 3,3′-dimethylnaphtidine in a stopped-flow injection system[66] to 20 μg L^{-1} for the direct spectrophotometric determination of V between pH 4.0 and 5.5 with 1,5-diphenylcarbohydrazide.[67]

Compared with these organic fluorophores, the Ru- and Re-based luminophores in $[Ru(bpy)_2(\mathbf{H_2\text{-}L^3})]^{2+}$ and $[ReBr(CO)_3(\mathbf{H_2\text{-}L^3})]$ have longer luminescence lifetimes and larger differences between the absorption and emission maxima. These photophysical properties are of advantage in the investigation of biological samples, since they can be used to discriminate the signal against background fluorescence.

Competition Studies. To assess the practicability of $[Ru(bpy)_2(\mathbf{H_2\text{-}L^3})]^{2+}$ and $[ReBr(CO)_3(\mathbf{H_2\text{-}L^3})]$ as chemosensors, their ability to detect molybdate in the presence of potentially competing ions was investigated at pH levels of 3 and 4, respectively. For this purpose, a stoichiometric quantity of the competing ions was added to the sensor solutions prior to the addition of molybdate. The emission intensity at 610 or 605 nm was then recorded 3 min after each addition. Figure 16 shows the observed decrease of emission intensity in comparison to the emission intensity of the free sensors.

(61) Seifter, S.; Novic, B. *Anal. Chem.* **1951**, *23*, 188.
(62) Blanco, C. C.; Campana, A. G.; Barrero, F. A.; Ceba, M. R. *Anal. Chim. Acta* **1993**, *283*, 213.
(63) Pal, B. K.; Singh, K. A.; Dutta, K. *Talanta* **1992**, 971.
(64) Jiang, C.; Wang, J.; He, F. *Anal. Chim. Acta* **2001**, *439*, 307.
(65) Agnihotri, N.; Dass, R.; Mehtra, J. R. *Anal. Sci.* **1999**, *15*, 1261.
(66) Palomeque, M. E.; Lista, A. G.; Band, B. S. F. *Anal. Chim. Acta* **1998**, *366*, 287.
(67) Ahmed, N. J.; Banoo, S. *Talanta* **1999**, *48*, 1085.

While the addition of most ions causes only small variations of the emission intensity of the sensors, the addition of Cu(II) causes a drop to ca. 80% of the original intensity in both cases. This drop is consistent with the effect that was observed for copper in the corresponding pH profiles.

The subsequent addition of molybdate to the solutions that already contain the competing ions results in the emission intensity falling to ca. 40% of the original intensity level of $[Ru(bpy)_2(\mathbf{H_2\text{-}L^3})]^{2+}$ and to ca. 5% of the intensity level of $[ReBr(CO)_3(\mathbf{H_2\text{-}L^3})]$. This decrease is in accordance with the residual emission intensities expected from the corresponding pH profiles in the presence of molybdate at pH levels 3 and 4, respectively. It can therefore be concluded that none of the competing ions tested affects the molybdate-binding ability of $[Ru(bpy)_2(\mathbf{H_2\text{-}L^3})]^{2+}$ and $[ReBr(CO)_3(\mathbf{H_2\text{-}L^3})]$ if present in concentrations equal to those of molybdate. However, Cu(II) and, in the case of $[ReBr(CO)_3(\mathbf{H_2\text{-}L^3})]$, Fe(III) may give rise to false positives in the absence of molybdate if the pH dependence is not further investigated.

The practicability of $[Ru(bpy)_2(\mathbf{H_2\text{-}L^3})]^{2+}$ and $[ReBr(CO)_3(\mathbf{H_2\text{-}L^3})]$ in the analysis of vanadate in the presence of potentially competing ions was also investigated. As evident from Figure 17, vanadate still quenches the emission of both sensors in the presence of competing ions. While the approximately 35% decrease in the emission intensity of $[ReBr(CO)_3(\mathbf{H_2\text{-}L^3})]$ upon the addition of vanadate is consistent with the residual intensity at pH 4 in the pH profile, the emission quenching of $[Ru(bpy)_2(\mathbf{H_2\text{-}L^3})]^{2+}$ appears to be less complete. From the pH profile, a decrease of ca. 60% of the intensity of free $[Ru(bpy)_2(\mathbf{H_2\text{-}L^3})]^{2+}$ is expected. In contrast, the intensity decrease observed in the presence of the competing ions varies considerably and averages only ca. 30%. This observation suggests that the solutions have not reached equilibrium after 3 min, when the emission intensity was recorded. Similar delays were not observed in the competition study with $[ReBr(CO)_3(\mathbf{H_2\text{-}L^3})]$ since the solutions were far more concentrated and the reaction rates were higher. The conditions used in the competition study with the Re-based sensor are thus more suitable for high-throughput analyses.

Summary and Conclusions

Two new luminescent chemosensors for biologically relevant oxometalates have been synthesized and characterized, and their spectroscopic properties have been studied. Since the sensors contain the same catecholamide receptor unit but different luminophores, the impact of the luminophore on the sensor properties could be investigated. The crystal structures of the sensors demonstrate that the conformation of $\mathbf{H_2\text{-}L^3}$ in the solid state does not change significantly on moving from a $[ReBr(CO)_3(phen)]$- to a $[Ru(bpy)_2(phen)]^{2+}$-type luminophore. Spectrophotometric titrations, however, show that the pK_a value of the 2-hydroxy-group is significantly lower in $[Ru(bpy)_2(\mathbf{H_2\text{-}L^3})]^{2+}$. Consequently, the optimum working pH for this sensor is lower that that for $[ReBr(CO)_3(\mathbf{H_2\text{-}L^3})]$.

$[Ru(bpy)_2(\mathbf{H_2\text{-}L^3})]^{2+}$ and $[ReBr(CO)_3(\mathbf{H_2\text{-}L^3})]$ both signal the presence and concentration of molybdate and vanadate through a decrease in emission intensity. In addition, $[ReBr(CO)_3(\mathbf{H_2\text{-}L^3})]$ also detects tungstate. The sensitivity for molybdate achieved with $[Ru(bpy)_2(\mathbf{H_2\text{-}L^3})]^{2+}$ is almost an order of magnitude higher than the one reached with $[ReBr(CO)_3(\mathbf{H_2\text{-}L^3})]$ and 3 orders of magnitude higher than the one published for the colorimetric determination of molybdate with catechol. Linking the catechol-based receptor unit to the metal-based luminophore brought the detection limits for molybdate and vanadate down to a level that falls within the range reported for highly fluorescent organic chromophores. In contrast to most organic fluorescent reagents, the $[ReBr(CO)_3(phen)]$- and $[Ru(bpy)_2(phen)]^{2+}$-type luminophores have long luminescence lifetimes and emission maxima at >600 nm. These properties could be used to discriminate the signal against biological background fluorescence.

Our approach allowed us to combine the photophysical advantages of the luminophores with the excellent selectivity of the catecholamide-based receptor unit for molybdate, tungstate, and vanadate. Due to the profound influence of the luminophore on the sensitivity, acid−base, and metal-binding properties of the chemosensors, Ru and Re complexes of this type have the potential to be tuned to suit particular applications by the selection of appropriate photophysical properties and charge of the luminophore.

Acknowledgment. We thank Prof. R. N. Perutz and Dr. N. Reddig for helpful discussions, the EPSRc National Mass Spectrometry Service Centre in Swansea for the HR mass spectra and the EPSRC [GR/R16464/01] for financial support.

Note Added after ASAP Publication. This article was released ASAP on July 6, 2007 with errors in Figures 16 and 17 where the Re complex should not have shown a positive charge. The correct version was posted on July 13, 2007.

Supporting Information Available: X-ray crystallographic data in CIF format and Figures S1−S11 are available free of charge via the Internet at http://pubs.acs.org. In addition, CCDC files 648122 and 648123 contain the crystallographic data. These data can be obtained free of charge from The Cambridge Crystallographic Data Centre via www.ccdc.cam.ac.uk/data_request/cif.

IC700554N